# Heat Flow Measurements

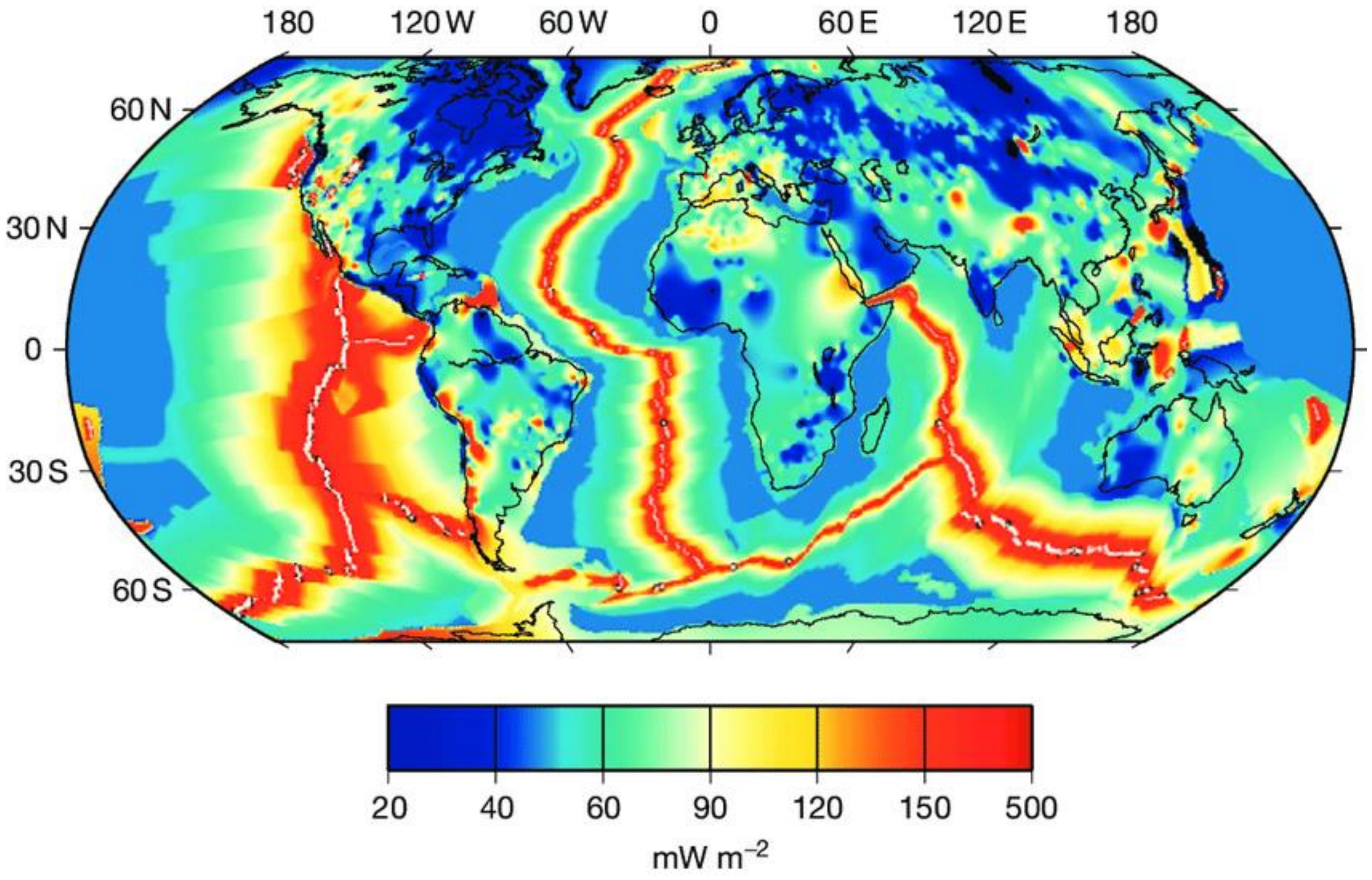


Daniel Gunning

# What is heat flow?

Heat flow is the movement of heat (or energy) from the interior of the Earth to the surface.

**Units:** mW / m2 (milliwatts per metre squared)

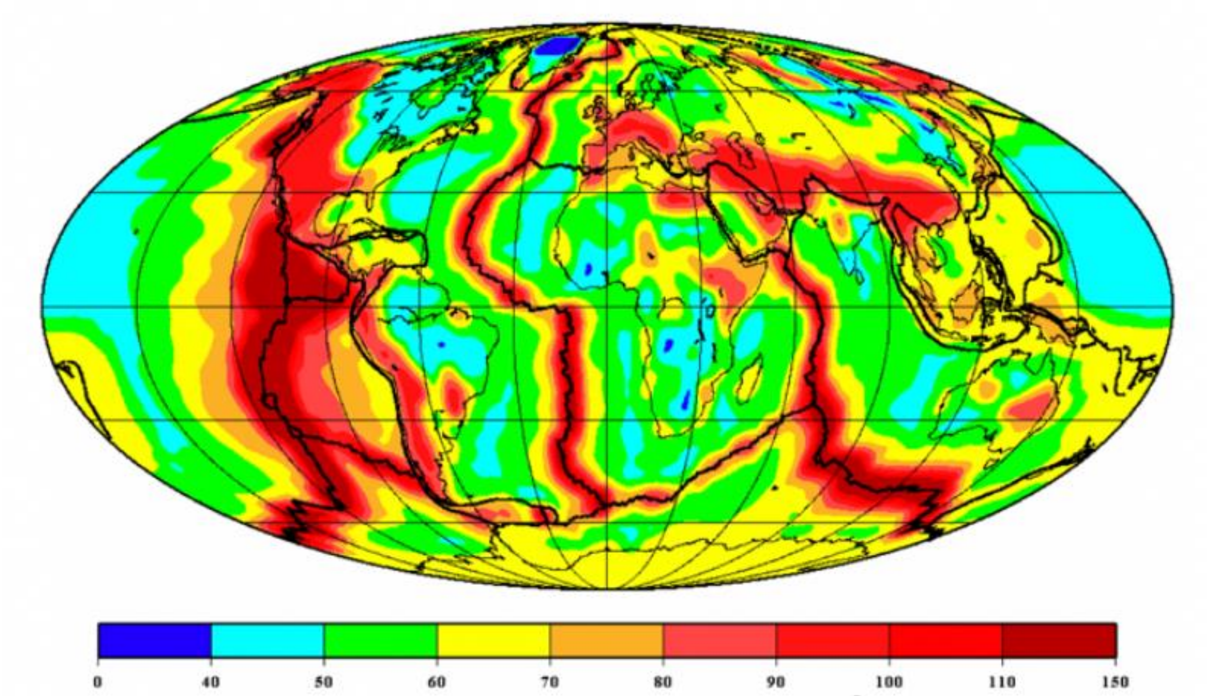


Global representation of heat flow based on observational datasets and supplemented with estimated derived from empirical correlations with age (Vieira and Hamza, 2018)

# The sources of heat flow

In steady-state conditions, heat flow ($\boldsymbol{Q}$) of the Earth is equal to (Jaupart, 2007)

$$\boldsymbol{Q} = \boldsymbol{Q}_{\boldsymbol{crust}} + \boldsymbol{Q}_{\boldsymbol{lith}} + \boldsymbol{Q}_{\boldsymbol{b}}$$

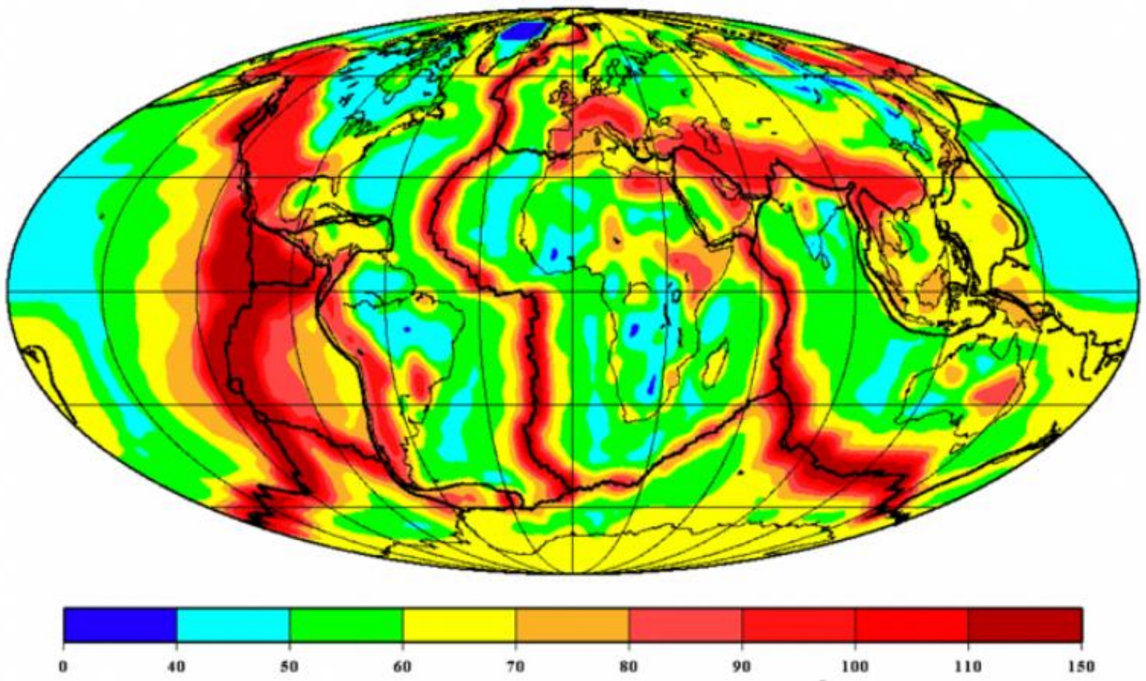


Global representation of heat flow based on observational datasets and supplemented with estimated derived from empirical correlations with age (Vieira and Hamza, 2018)

- Heat production from the crust ($\boldsymbol{Q}_{\boldsymbol{crust}}$) and the lithospheric mantle ($\boldsymbol{Q}_{\boldsymbol{lith}}$) is derived from the radioactive decay of U, Th and K in silicate rocks.
- Heat flux at the base of the lithosphere ($\boldsymbol{Q}_{\boldsymbol{b}}$) from the convection of the mantle.
- Also, there is transient cooling from major tectonic events or magmatic perturbations (especially for ocean crust)

# Heat flow in oceanic crust

Oceanic heat flows are higher (~101 mW/m2) than continental crust (~65 mW/m2) due to transient cooling.

Oceanic crust does not contain much radioactive elements.

Ocean heat fluxes decrease with age but stagnate around 120 million years ago.

There is high variability in measured ocean heat fluxes for young oceanic crust which has been linked hydrothermal circulation.

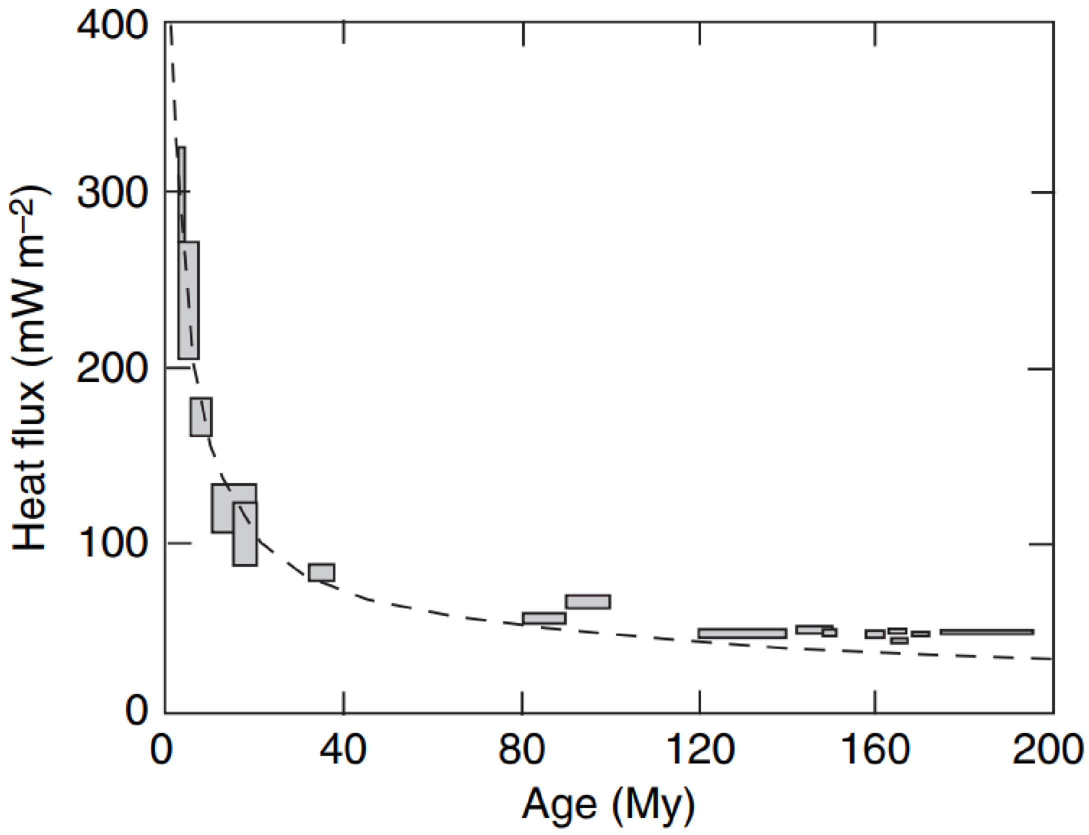


Ocean heat flux data as a function of age (Jaupart and Mareschal, 2007)

# Heat flow in continental crust

Crustal heat production (from the decay of radioactive elements) is the largest contributor to heat flow in continental crust.

Age is not a good proxy for heat flow in continental crust

Crustal heat production can account for regional variations in heat flow

Higher heat flow is associated a radioactively enriched layer of upper crust.

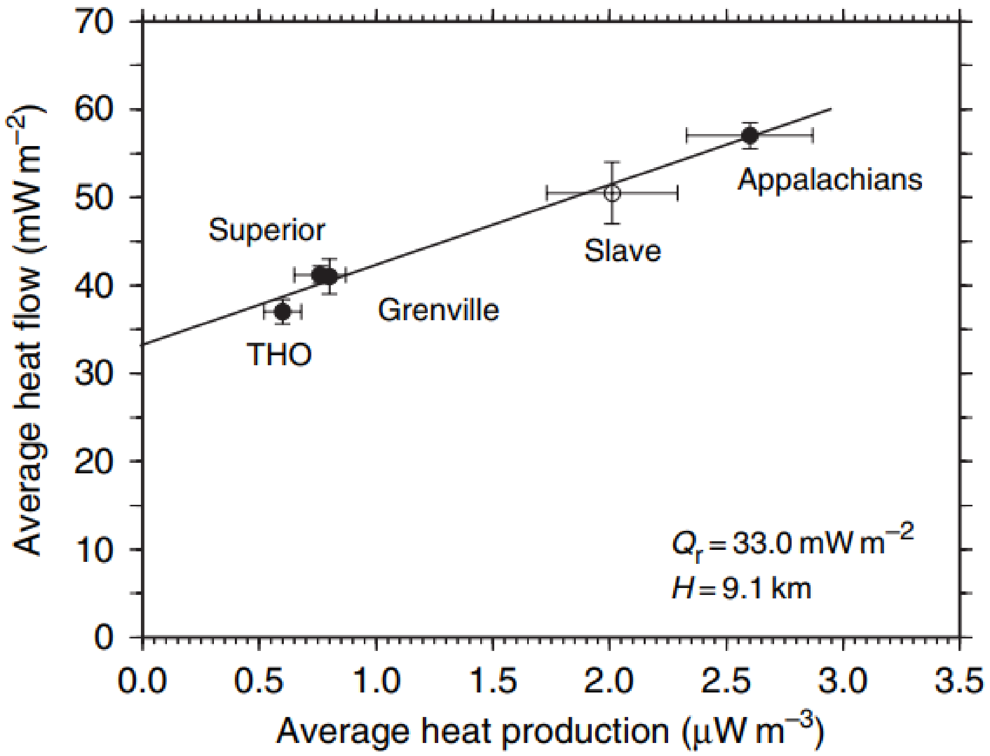


Average heat flow plotted against average heat production for geological provinces in North America (Jaupart and Mareschal, 2007)

# How is heat flow measured?

**Heat flow is not measured directly !**

Heat flow (**Q**) is calculated as the product of the thermal conductivity (**K**) and the temperature gradient (**T**).

$$\mathbf{Q = -T.K.}$$

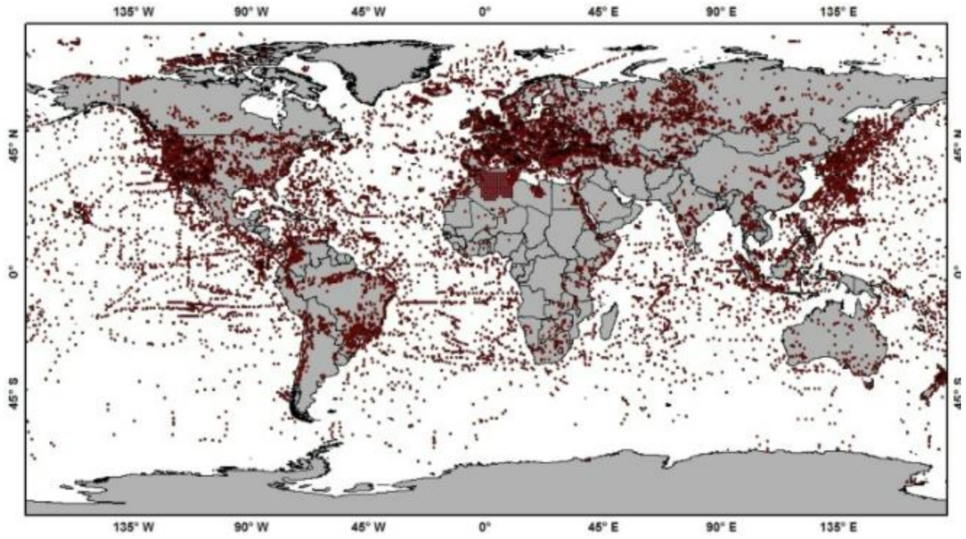


Location of heat flow measurements (Vieira and Hamza (2018)

To obtain values of thermal conductivity and temperature gradients we need boreholes!

# How is the thermal conductivity obtained?

Thermal conductivity is the property of a materials ability to conduct heat.

Thermal conductivity varies with rock composition, texture and temperature.

**Units**: W/K.m (watts per kelvin-meter)

There are three common methods for measuring thermal conductivity in the laboratory:

1. **Divided Bar Method**
2. **Transient Line Method**
3. **Optical Scanning**

**Table 6** Thermal conductivity of some rocks at room temperature

| Rock type | Mean ($W\,m^{-1}\,K^{-1}$) | Min–max ($W\,m^{-1}\,K^{-1}$) | References |
|---|---|---|---|
| Basalt | 2.0 | 1.8–2.5 | Clark (1966) |
| Gabbro | 2.2 | 1.8–2.5 | Clark (1966) |
| Gneiss | 3.6 | 2.0–5.0[a] | Clauser and Huenges (1995) |
| Granite | 3.2 | 2.8–3.6 | Clark (1966) |
| Granulite facies rocks | — | 3.01–3.48 | Joeleht and Kukkonen (1998) |
| Peridotite | 2.8 | 2.3–3.4 | Clark (1966) |

[a]Thermal conductivity of gneiss in direction perpendicular to foliation is 0.6 that parallel to foliation.

Jaupart and Mareschal, 2004

# Method 1: Divided Bar (Steady-State)

A disk of rock sampled from the borehole is placed between metal bars, which is heated from the top and cooled at the bottom until heat flow is constant.

In steady-state conditions:

Heat flow

$$\mathbf{Q = -T.K}$$

Steady state

$$-T_R K_R = -T_B K_B$$

If we know the temperature gradients of the rock specimen **(-$T_R$)** and the bar **(-$T_A$)**, in addition to the thermal conductivity of the bar **($K_B$), we** can solve for the thermal conductivity of the rock sample **($K_R$)**

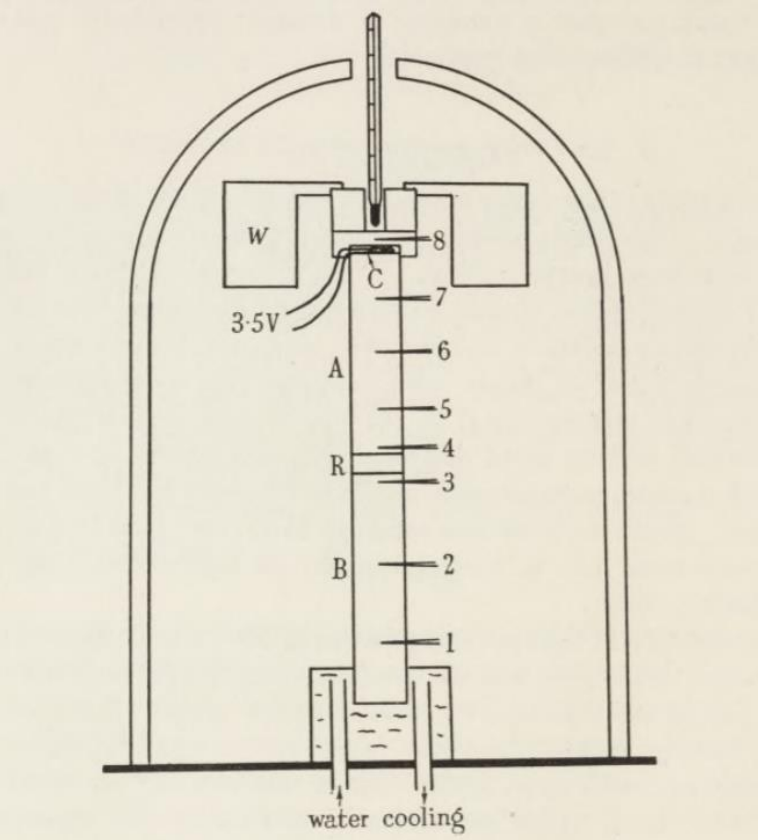


FIGURE 1. Diagram of the rock conductivity apparatus.

Diagram of the divided bar apparatus (Benfield, 1939)

# Method 2: Transient line source method

Common line source methods involve need probes, inserted into unconsolidated or consolidated rocks with a thermistor in the centre to record the temperature rise

The sample is heated and the sensor monitors temperature rise as a function of time of the material and this slope can be directly related to thermal conductivity.

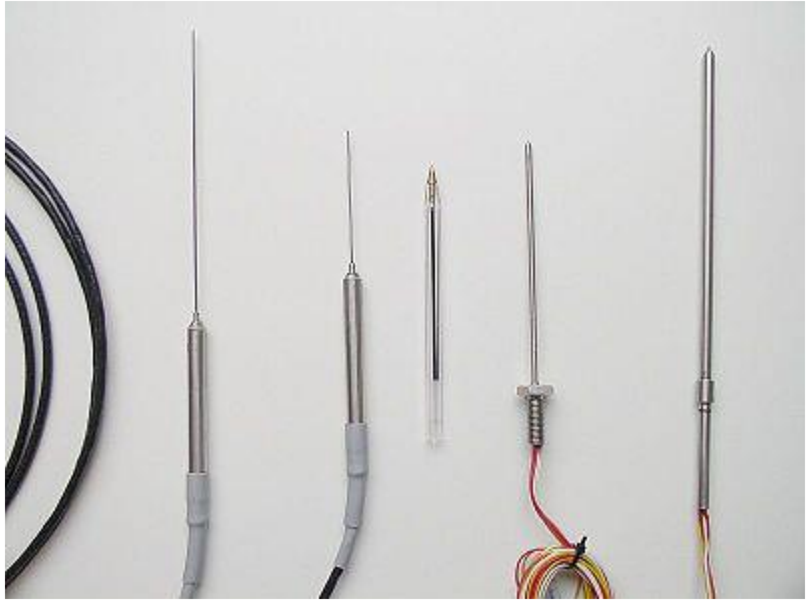

Examples of needle probes inserted into rock samples

# Method 3: Optical scanning

Yuri Popov developed rapid and non-destructive method for measuring thermal conductivity for large numbers of rocks

A device containing a laser heat source and infrared thermometer moved across the surface of rock samples. Measures the maximum temperature increase (Θ).

The thermal conductivity of each sample is determined using the thermal conductivity of the reference sample (Kr) and the ratio of ΘR to Θ.

$$K = K_R . \frac{\Theta_R}{\Theta}$$

The deviation of results from these three techniques less than 4% (Popov et al., 1999).

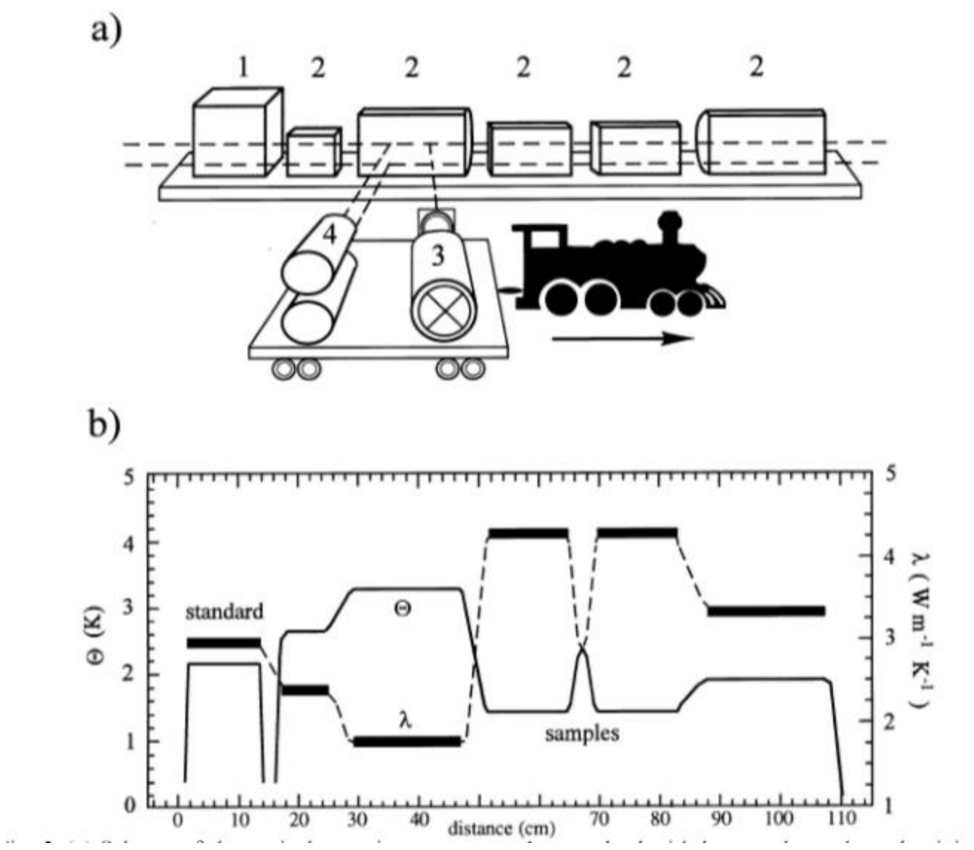


a) Scheme of the optical scanning apparatus and b) relationship between max temperature rise and thermal conductivity (Poppov et al., 1999)

# How is temperature gradients measured?

Electronic thermometers deployed on steel or alloy wires which are lowered into the borehole to measure temperatures within the Earth.

The measurement of temperatures usually involves transducers – which convert variations in a physical quantity into an electric signal (these include **thermistors, platinum resistance elements, diodes and fibre optics**)

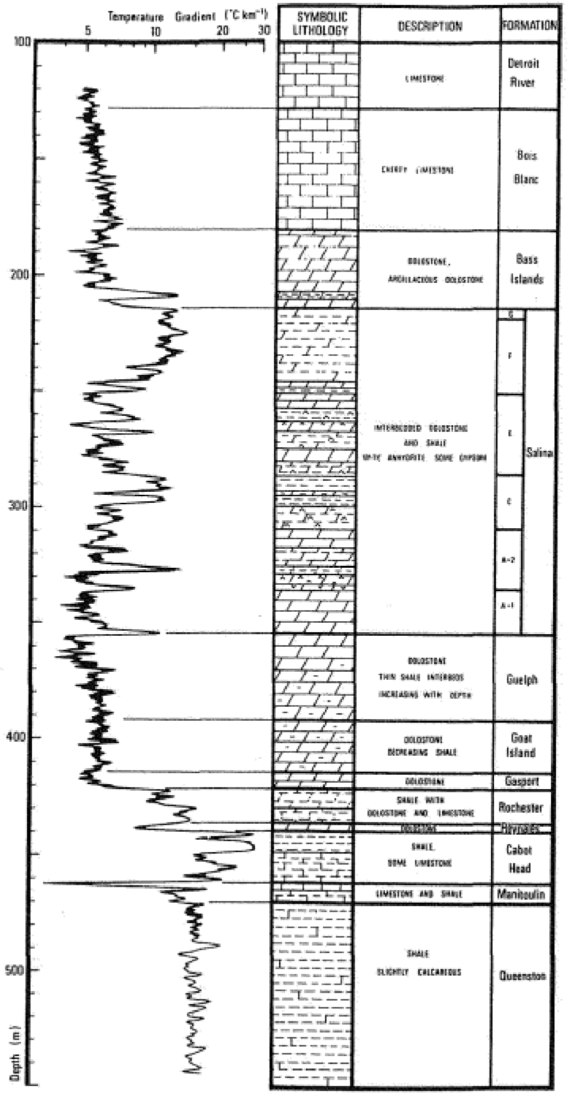


Example temperature gradient log

# The first ever measurement of heat flow

Everett (1883) compiled temperature gradient measurements from mines and boreholes across the world. The average thermal conductivity from a variety of rock types were calculated (e.g. rock salts, granites, clays, sandstones, etc.). These two values were multiplied to determine average heat flow of the outer crust

The first modern measurements of continental heat flow was during the 1930s in Britain (Benfield, 1939) and South Africa (Bullard, 1939). Modern entails temperature gradients and thermal conductivity measurements from the same borehole

The first modern measurements of heat flow in the oceans was the 1950s (Revelle and Maxwell, 1952)

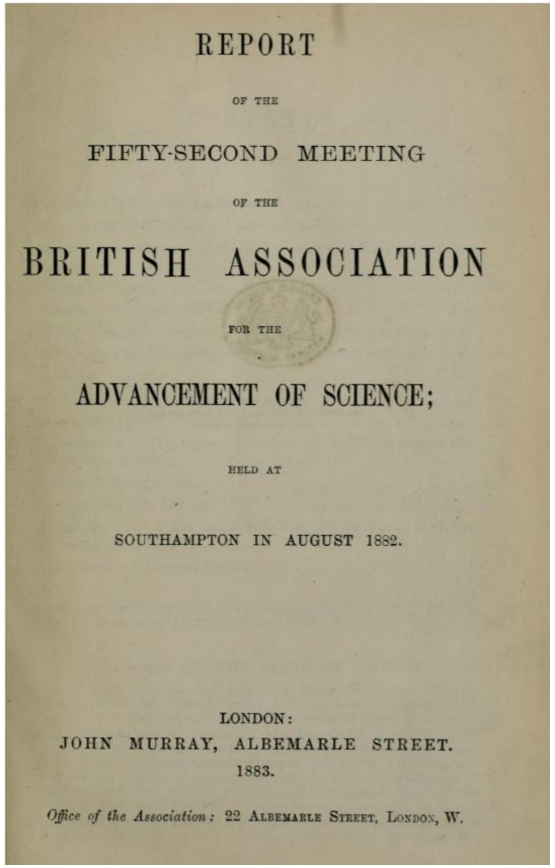
REPORT

OF THE

FIFTY-SECOND MEETING

OF THE

BRITISH ASSOCIATION

FOR THE

ADVANCEMENT OF SCIENCE;

HELD AT

SOUTHAMPTON IN AUGUST 1882.

LONDON:
JOHN MURRAY, ALBEMARLE STREET.
1883.

*Office of the Association:* 22 ALBEMARLE STREET, LONDON, W.

(Everett, 1883)

# Calculation of heat flow

Commonly one of two methods to calculate heat flow

**Method 1: Combination of mean thermal conductivity with temperature gradient**

Method 2: The “Bullard plot”

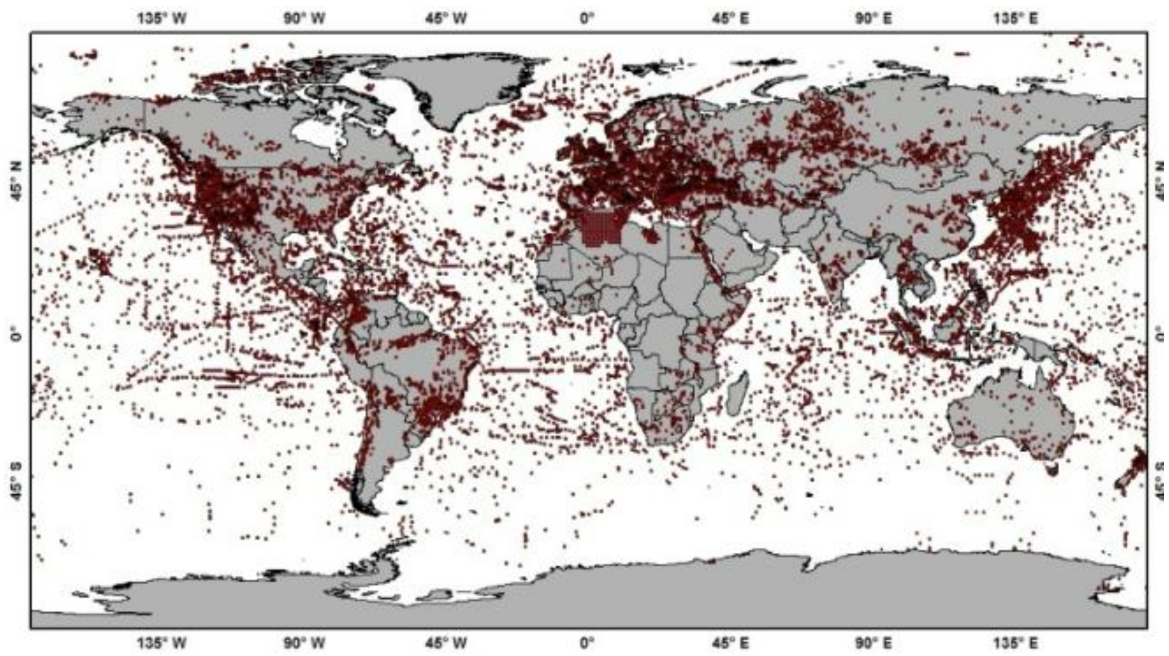


Location of heat flow measurements (Vieira and Hamza (2018)

# Example of heat flow calculations using method 1

Mareschal et al., (2004) carried out heat flow calculations in the Slave province of the Canadian Shield in northwest Canada .

Two geotechnical boreholes (300-400 m depth) in diamond mines

$$\mathbf{Q} = -\mathbf{T}.\mathbf{K}.$$

**Temperature gradient (T):** 15 cemented thermistors placed in the borehole and the data was regularly gathered.

**Thermal conductivity:** Rock samples from the borehole (or neighbouring boreholes) using the divided bar method.

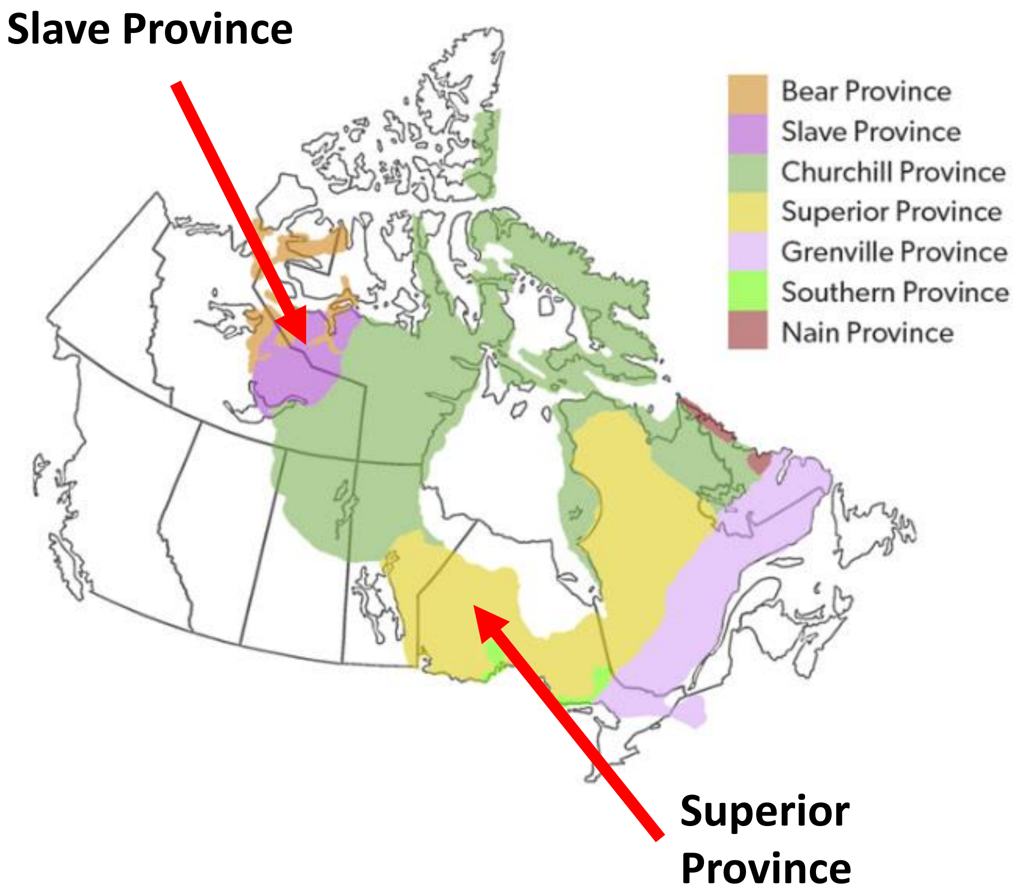

# Example of heat flow calculations using method 1

Average heat flow (Q) using a constant thermal conductivity was 43 and 48 mW/m2 for the Lac de Gras boreholes.

Heat flows were found to higher in the Slave province compared with the Superior province of the Canadian Shield due to higher crustal heat production

Three layer crustal model indicated the radioactive decay of elements accounted for 34 mW/m2 of heat flow, leaving 12 mW/m2 for mantle flow

**Lac de Gras borehole measurements**

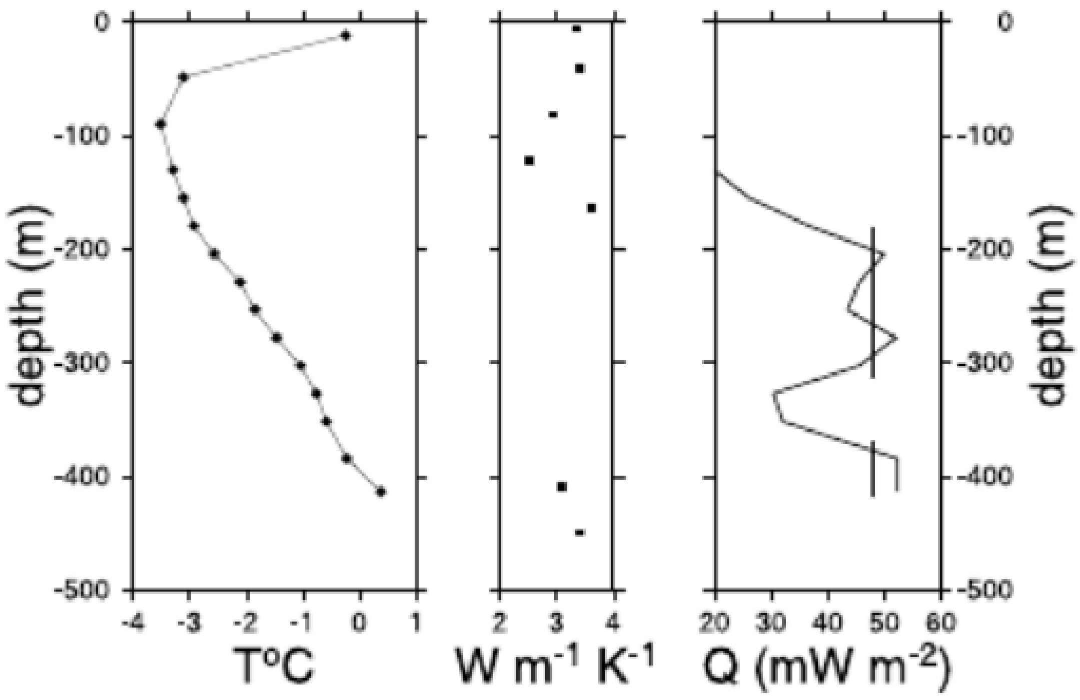


Temperature profile, thermal conductivity and heat flow (Mareschal et al., 2004)

# Calculation of heat flow

Commonly one of two methods to calculate heat flow

Method 1: Combination of mean thermal conductivity with temperature gradient

**Method 2: The "Bullard plot"**

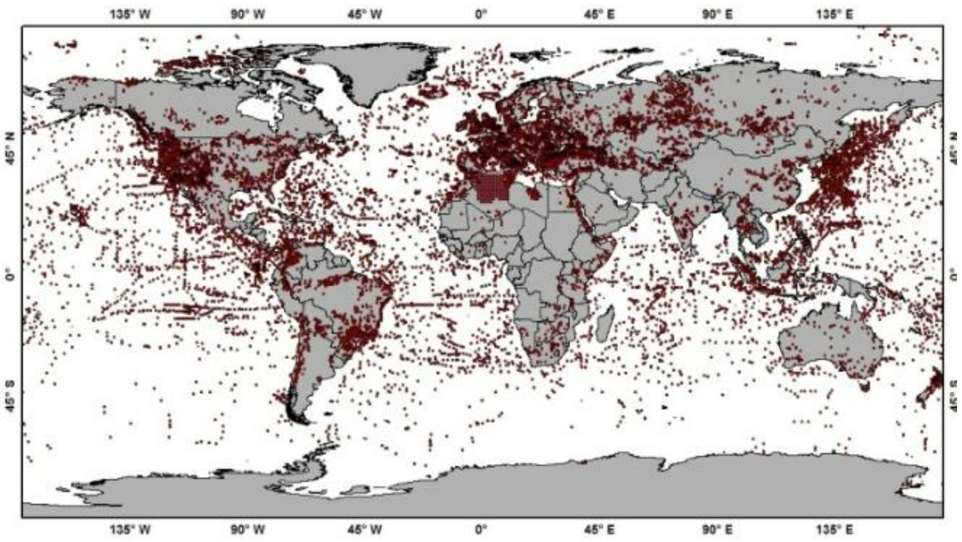


Location of heat flow measurements (Vieira and Hamza (2018)

# Method 2: Bullard Plot

Bullard plot: The temperature plotted against the thermal resistivity

Thermal resistivity is the thickness of the lithological unit divided by the thermal conductivity .

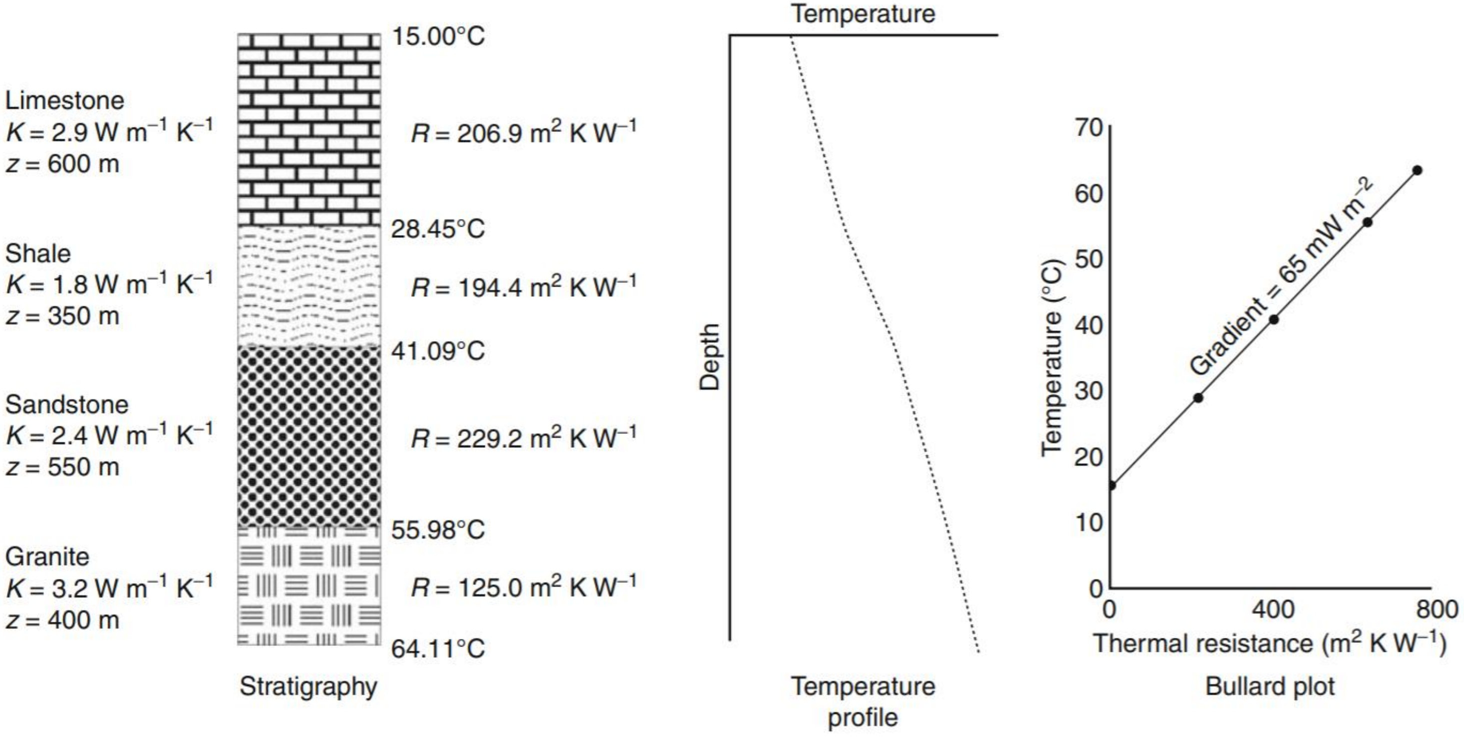


A depiction of rock sequences with thermal properties and unit thicknesses (left), the temperature with depth (right) in the borehole, and the Bullard plot of temperature with thermal resistance (right)

For boreholes with significant thermal conductivity stratification, Bullard plots are most appropriate

The best fit slope of the Bullard plot is the heat flow from the borehole.

# In-Situ Methods of calculating heat flow

The recovery of rock samples is high cost and difficult, especially for unconsolidated material.

There are now several methods for calculating thermal conductivity, temperature gradient and heat flow in situ and during the drilling process, without requiring rock samples or laboratories.

Friefeld et al., (2008) determined thermal conductivity of an entire borehole at a 1m resolution by coupling temperature gradient measurements with a line source heating loop

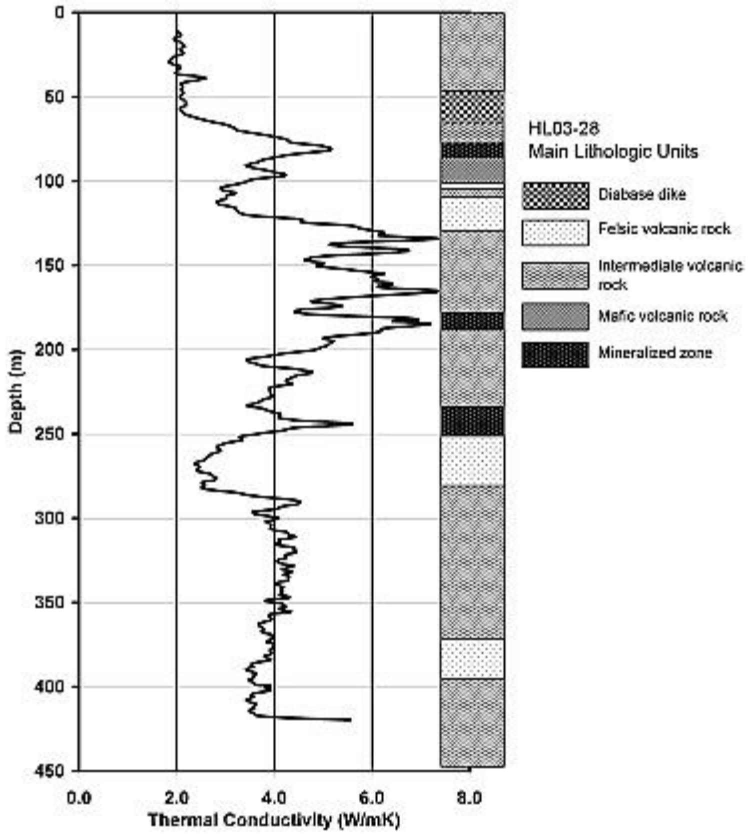


In-situ thermal conductivity measurements as a function of depth (Friefeld et al., 2008)

# Global Heat Flow Databases

The number of heat flow measurements is always increasing

| Authors | Heat Flow measurements |
|---|---|
| Chapman and Pollack (1980) | 7,217 |
| Pollack et al., (1993) | 20,201 |
| Davies and Davies (2010) | 38,347 |
| Vieira and Hamza (2018) | 44, 386 |

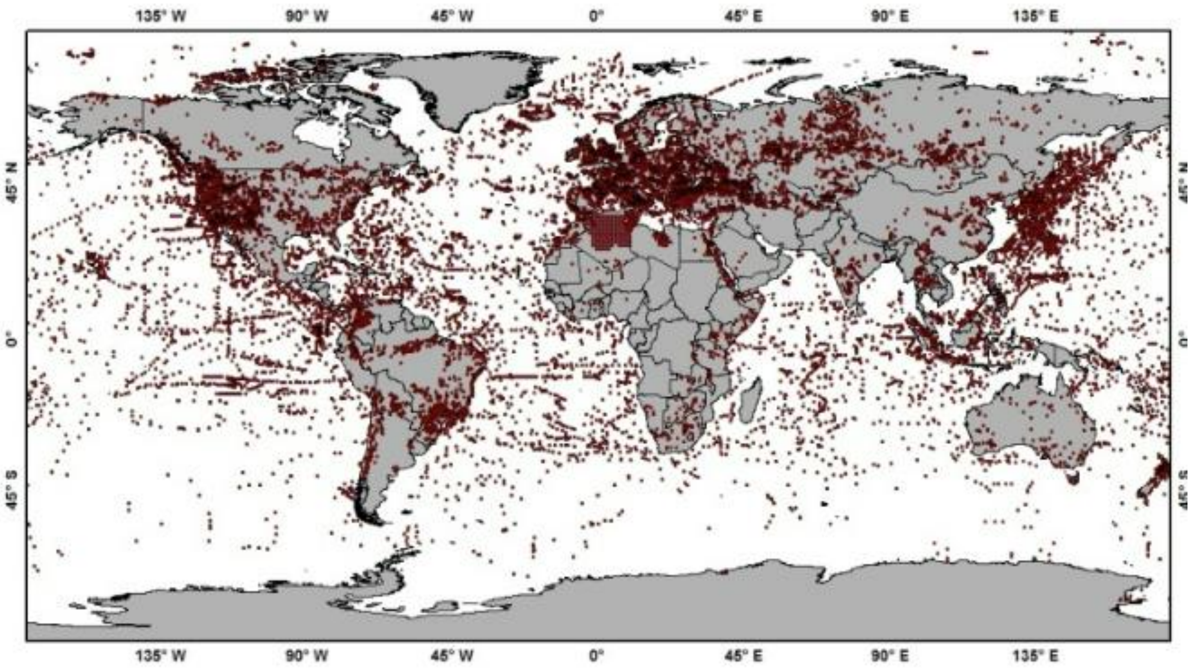


Location of heat flow measurements (Vieira and Hamza (2018)

However, these are still sparse and non-uniformly distributed …

# Global Heat Flow Databases - extrapolation

Most studies determine empirical relationship between tectonic age and the average heat flow.

Heat flow measurements can then be assigned to regions with no observations

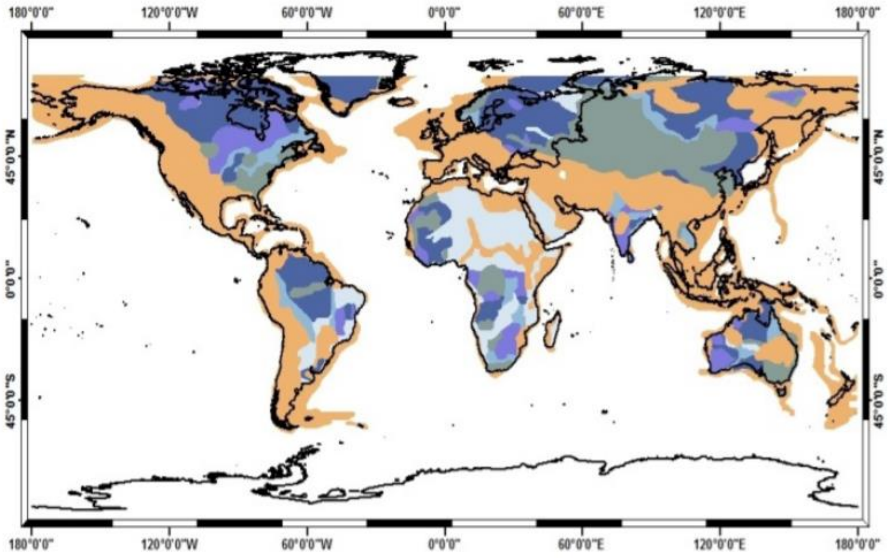


Map of tectonic units (Vieira and Hamza, 2018)

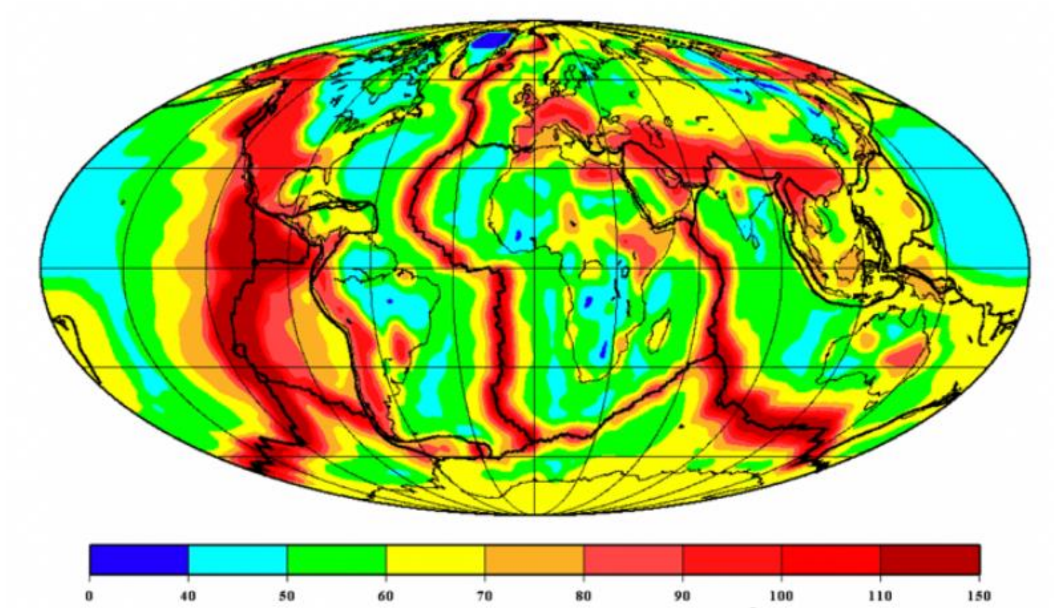


Global representation of heat flow based on observational datasets and supplemented with estimated derived from empirical correlations with age (Vieira and Hamza, 2018)

# Alternative method: Airborne magnetic anomalies

Based on the fact ferromagnetic materials lose their magnetism once they reach the Curie temperature.

For magnetite (the dominant ferromagnetic material in the Earth's crust), it is the 580C isotherm.

Martos et al., (2017) compiled magnetic anomalies from airborne surveys and satellite data to determine the depth of the deepest magnetic source underneath Antarctica

$$\mathbf{Q} = -\mathbf{T}.\mathbf{K}$$

Temperature gradient from the curie depth of the 580 isotherm and the surface (0C).

Constant thermal conductivity of 2.8 W/mK.

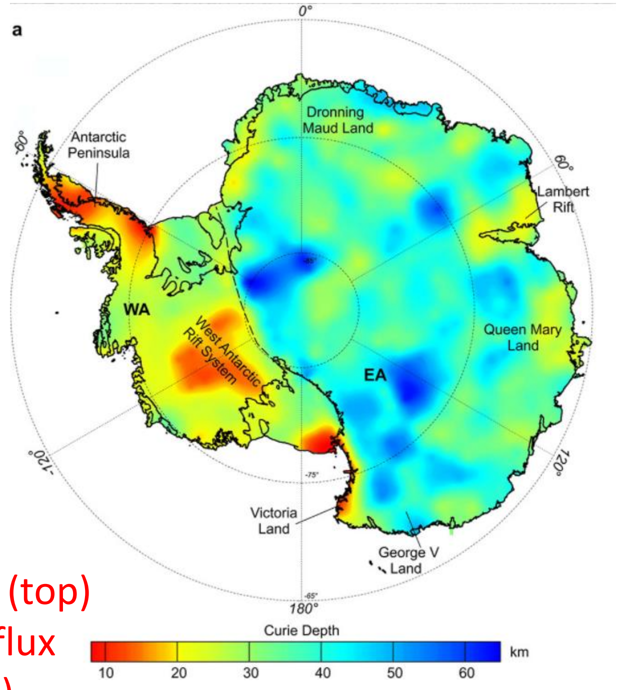


Curie depth (top) and heat flux bottom) (Martos et al., 2017)

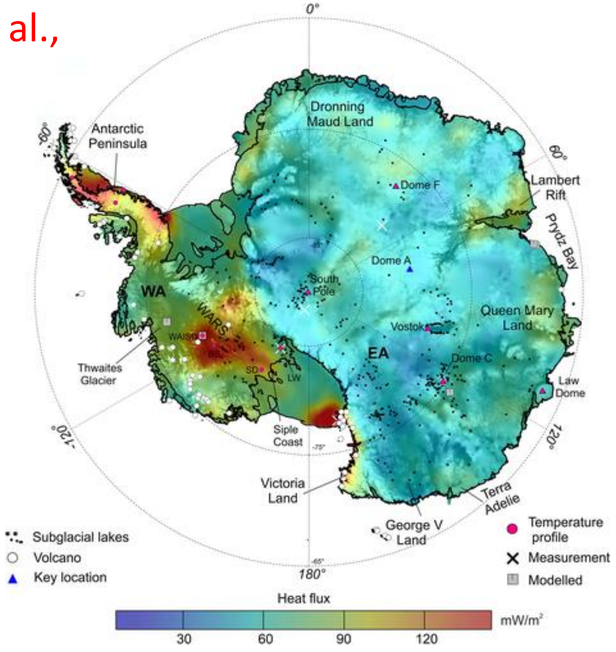

# References

Hamza, V. & Vieira, Fábio. (2018). Global Heat Flow: New Estimates Using Digital Maps and GIS Techniques. International Journal of Terrestrial Heat Flow and Applications. 1. 6-13. 10.31214/ijthfa.v1i1.6.

Sass J.H., Beardsmore G. (2011) Heat Flow Measurements, Continental. In: Gupta H.K. (eds) Encyclopedia of Solid Earth Geophysics. Encyclopedia of Earth Sciences Series. Springer, Dordrecht. https://doi.org/10.1007/978-90-481-8702-7_72

Jaupart, C. & Mareschal, jean-claude. (2007). 6.05 Heat Flow and Thermal Structure of the Lithosphere. 10.1016/B978-044452748-6/00104-8.

Popov, Y. A., Pribnow, D. F. C., Sass, J. H., Williams, C. F., and Burkhardt, H., 1999. Characterization of rock thermal conductivity by high-resolution optical scanning. Geothermics, 28, 253–276

Freifeld, B. M., Finsterle, S., Onstott, T. C., Toole, P., and Pratt, L. M., 2008. Ground surface temperature reconstructions: using in situ estimates for thermal conductivity acquired with a fiber-optic distributed thermal perturbation sensor. Geophysical Research Letters, 35, L14309, doi:10.1029/2008GL034762

Freifeld, B. M., Finsterle, S., Onstott, T. C., Toole, P., and Pratt, L. M., 2008. Ground surface temperature reconstructions: using in situ estimates for thermal conductivity acquired with a fiber-optic distributed thermal perturbation sensor. Geophysical Research Letters, 35, L14309, doi:10.1029/2008GL034762

Martos, Y. M., Catalán, M., Jordan, T. A., Golynsky, A., Golynsky, D., Eagles, G., & Vaughan, D. G. (2017). Heat flux distribution of Antarctica unveiled. Geophysical Research Letters, 44,11, 417–11,426. https://doi.org/10.1002/2017GL075609